The Astrophysical Journal, 837:144 (16pp), 2017 March 10 https://doi.org/10.3847/1538-4357/837/2/144

On the Redshift of TeV BL Lac Objects

Simona Paiano[1,2], Marco Landoni[2], Renato Falomo[1], Aldo Treves[3], Riccardo Scarpa[4], and Chiara Righi[2,3]
[1] INAF, Osservatorio Astronomico di Padova, Vicolo dell'Osservatorio 5 I-35122 Padova (PD), Italy
[2] INAF, Osservatorio Astronomico di Brera, Via E. Bianchi 46 I-23807 Merate (LC), Italy
[3] Università degli Studi dell'Insubria, Via Valleggio 11 I-22100 Como, Italy
[4] Instituto de Astrofisica de Canarias, C/O Via Lactea, s/n E38205—La Laguna (Tenerife), Espana
Received 2016 November 17; revised 2017 January 10; accepted 2017 January 14; published 2017 March 13

Abstract

We report results of a spectroscopic campaign carried out at the 10 m Gran Telescopio Canarias for a sample of 22 BL Lac objects detected (or candidates) at TeV energies, aiming to determine or constrain their redshift. This is of fundamental importance for the interpretation of their emission models and for population studies and is also mandatory for studying the interaction of high-energy photons with the extragalactic background light using TeV sources. Optical spectra with high signal-to-noise ratios in the range 4250–10000 Å were obtained to search for faint emission or absorption lines from both the host galaxy and the nucleus. We determine a new redshift for PKS 1424+240 ($z = 0.604$) and a tentative one for 1ES 0033+595 ($z = 0.467$). We are able to set new spectroscopic redshift lower limits for three other sources on the basis of Mg II and Ca II intervening absorption features: BZB J1243+3627 ($z > 0.483$), BZB J1540+8155 ($z > 0.672$), and BZB 0J2323+4210 ($z > 0.267$). We confirm previous redshift estimates for four blazars: S3 0218+357 ($z = 0.944$), 1ES 1215+303 ($z = 0.129$), W Comae ($z = 0.102$), and MS 1221.8+2452 ($z = 0.218$). For the remaining targets, in seven cases (S2 0109+22, 3C 66A, VER J0521+211, S4 0954+65, BZB J1120+4214, S3 1227+25, BZB J2323+4210), we do not validate the proposed redshift. Finally, for all sources of still-unknown redshift, we set a lower limit based on the minimum equivalent width of absorption features expected from the host galaxy.

Key words: BL Lacertae objects: general – galaxies: distances and redshifts – gamma rays: galaxies – quasars: absorption lines – quasars: emission lines

1. Introduction

Blazars are luminous emitters over the whole electromagnetic spectrum up to TeV energies. They are highly variable and polarized and are often dominated, especially during outbursts, by gamma-ray emission. The standard paradigm for these sources is that they owe their extreme physical behavior to the presence of a relativistic jet closely aligned with the observer's direction, a model that explains most of the peculiar properties of these sources: superluminal motion, rapid variability, huge radio brightness temperature, and so on. From the optical point of view, blazars showing very weak lines or completely featureless spectra are named BL Lac objects (BLLs; see, e.g., the review of Falomo et al. 2014).

Compared to other active galactic nuclei, the featureless spectrum of BLLs is due to the extreme dominance of the nonthermal emission over the stellar emission of the host galaxy, which makes the assessment of their redshift very difficult (Sbarufatti et al. 2005b, 2006a, 2006b, 2009; Landoni et al. 2012, 2013, 2014, 2015; Shaw et al. 2013; Massaro et al. 2014, 2015; Álvarez Crespo et al. 2016).

Knowledge of the distance is, however, crucial to understanding the nature of these sources, the physical mechanism responsible for their extremely energetic emission, their intrinsic luminosity, and their cosmic evolution. Furthermore, in the case of TeV BLLs, the simple knowledge of the redshift converts these sources into a powerful probe of the extragalactic background light through γ–γ absorption, also improving our understanding of supersymmetric particles thought to be produced in their ultrarelativistic jets (see, e.g., Tavecchio et al. 2015). Thus, we undertook a spectroscopic observational campaign of a sample of TeV (or TeV candidate) BLLs with unknown or uncertain redshift to be observed at the 10.4 m Gran Telescopio Canarias (GTC), in order to improve our knowledge of the redshift of TeV BLLs, a possibly unique test bench for ultra-high-energy fundamental physics.

The first results of this program were presented in Landoni et al. (2015) for S4 0954+65 and in Paiano et al. (2016) for S2 0109+22. In this paper, we report results for 22 additional BLLs: 15 of them are detected at TeV energies, and seven are good TeV candidates (Massaro et al. 2013).

In Section 2 we outline the selection criteria of our sample and discuss their main properties. In Section 3 we present the data collection and the reduction procedure. In Section 4 we show the optical spectra of each object, underlying their main features, and discuss their redshift. In Section 5 we give detailed notes on individual objects, and finally in Section 6 we summarize and discuss the results.

In this work we assume the following cosmological parameters: $H_0 = 70$ km s^{-1} Mpc^{-1}, $\Omega_\Lambda = 0.7$, and $\Omega_m = 0.3$.

2. The Sample

We selected all BLLs that are detected at the very high energy band (>100 GeV) from the online reference catalog of TeV sources (TeVCAT[5]) with unknown or uncertain redshift and that are observable from La Palma ($\delta > -20°$). For objects with uncertain redshift, we chose sources with contrasting redshift values reported in the literature or with measurements from optical spectra of low signal-to-noise ratio. This selection yields 18 targets, and we obtain observations for 15 of them

[5] http://tevcat2.uchicago.edu/

Table 1
The Sample of Teraelectronvolt BL Lac and Teraelectronvolt Candidates

Object name	R.A. (J2000)	δ (J2000)	CLASS	V	$E(B-V)$	$z_{\rm literature}$	Reference
BZB J0035+1515	00:35:14.70	15:15:04.0	TeVc	16.9	0.062	?	⋯
1ES 0033+595	00:35:52.60	59:50:05.0	HBL	19.5	1.386	?	⋯
S2 0109+22[a]	01:12:05.08	22:44:39.0	IBL	15.7	0.034	0.265 ?	Healey et al. (2008)
RGB J0136+391	01:36:32.50	39:06:00.0	HBL	15.8	0.068	?	⋯
S3 0218+357	02:21:05.50	35:56:14.0	HBL[b]	20.0	0.061	0.944	Cohen et al. (2003)
3C 66A	02:22:39.60	43:02:08.0	IBL	15.0	0.075	0.444 ?	Miller et al. (1978)
VER J0521+211	05:21:45.90	21:12:51.0	IBL	17.5	0.604	0.108 ?	Shaw et al. (2013)
1ES 0647+250	06:50:46.50	25:03:00.0	HBL	15.7	0.087	?	⋯
S5 0716+714	07:21:53.40	71:20:36.0	IBL	15.5	0.027	?	⋯
BZB J0915+2933	09:15:52.40	29:33:24.0	TeVc	15.8	0.021	?	⋯
S4 0954+65[c]	09:58:47.20	65:33:55.0	LBL	17.0	0.106	0.367 ?	Lawrence et al. (1986)
BZB J1120+4212	11:20:48.00	42:12:12.0	TeVc	17.3	0.001	0.124 ?	Perlman et al. (1996)
1ES 1215+303	12:17:52.10	30:07:01.0	HBL	15.8	0.020	0.13 ?	Bade et al. (1998)
W Comae	12:21:31.70	28:13:59.0	IBL	15.4	0.021	0.102 ?	Weistrop et al. (1985)
MS 1221.8+2452	12:24:24.20	24:36:24.0	HBL	16.7	0.019	0.218 ?	Morris et al. (1991)
S3 1227+255	12:30:14.10	25:18:07.0	IBL	14.7	0.017	0.135 ?	Nass et al. (1996)
BZB J1243+3627	12:43:12.70	36:27:44.0	TeVc	16.2	0.010	?	⋯
BZB J1248+5820	12:48:18.80	58:20:29.0	TeVc	15.4	0.011	?	⋯
PKS 1424+240	14:27:00.40	23:48:00.0	HBL	14.6	0.050	?	⋯
BZB J1540+8155	15:40:15.80	81:55:06.0	TeVc	17.6	0.044	?	⋯
RGB J2243+203	22:43:54.70	20:21:04.0	HBL	16.0	0.042	?	⋯
BZB J2323+4210	23:23:52.10	42:10:59.0	TeVc	17.0	0.134	0.059 ?	Perlman et al. (1996)

Notes. Col. 1: Name of the target; Col. 2: Right ascension; Col. 3: Declination; Col. 4: Class of the source: high-synchrotron peaked BL Lac (HBL), intermediate-synchrotron peaked BL Lac (IBL), low-synchrotron peaked BL Lac (LBL), teraelectronvolt candidate BL Lac (TeVc); Col. 5: V-Band magnitudes taken from NED; Col. 6: $E(B-V)$ taken from the NASA/IPAC Infrared Science Archive (https://irsa.ipac.caltech.edu/applications/DUST/); Col. 7: Redshift; Col. 8: Reference to the redshift.

[a] Details for S2 0109+22 are reported in Paiano et al. (2016).

[b] Gravitationally lensed system.

[c] Details for S4 0954+65 are reported in Landoni et al. (2015).

(see Table 1), which represent about 70% of the whole sample of TeV blazars with uncertain or unknown redshift.

In addition, we selected BLLs from a sample of 41 objects[6] proposed as TeV emitters by Massaro et al. (2013) on the basis of the combined infrared (IR) and X-ray properties of BLLs reported in the ROMA-BZCAT catalog (Massaro et al. 2009), satisfying the criteria of uncertain redshift and observability. This selection produced 12 TeV candidates, and we obtained spectra for seven of them (see Table 1), which represent ∼60% of the unknown or uncertain TeV candidate emitters proposed by Massaro et al. (2013).

3. Observations and Data Reduction

Observations were obtained between 2015 February and 2016 August in Service Mode at the GTC using the low-resolution spectrograph OSIRIS (Cepa et al. 2003). The instrument was configured with the two grisms R1000B and R1000R,[7] in order to cover the spectral range 4000–10000 Å, and with a slit width = 1″, yielding a spectral resolution of $\lambda/\Delta\lambda = 800$.

For each grism, three individual exposures were obtained (with exposure times ranging from 300 to 1200 s each, depending on the source magnitude), which were then combined into a single average image, in order to perform optimal cleaning of cosmic rays and CCD cosmetic defects. Detailed information on the observations are given in Table 2.

Data reduction was carried out using IRAF[8] and adopting the standard procedures for long-slit spectroscopy with bias subtraction, flat-fielding, and bad-pixel correction. Individual spectra were cleaned of cosmic-ray contamination using the L. A. Cosmic algorithm (van Dokkum 2001).

Wavelength calibration was performed using the spectra of Hg, Ar, Ne, and Xe lamps, providing an accuracy of 0.1 Å over the whole spectral range. Spectra were corrected for atmospheric extinction using the mean La Palma site extinction table.[9] Relative flux calibration was obtained from the observations of spectrophotometric standard stars secured during the same nights as the target observation. For each object, the spectra obtained with the two grisms were merged into a final spectrum covering the whole desired spectral range.

Thanks to the availability of a direct image of the target, which is obtained at GTC as part of target acquisition, the spectra could be flux calibrated. The calibration was assessed using the zero point provided by the GTC-OSIRIS web page.[10] For one-half of our sample, it was also possible to use stars with known flux from the SDSS survey to double-check the flux calibration. We found no significant difference on average between the two methods within ∼0.1 mag. The final spectra

[6] One-h alf of them have unknown or uncertain redshift.

[7] http://www.gtc.iac.es/instruments/osiris/osiris.php

[8] IRAF (Image Reduction and Analysis Facility) is distributed by the National Optical Astronomy Observatories, which are operated by the Association of Universities for Research in Astronomy, Inc., under cooperative agreement with the National Science Foundation.

[9] https://www.ing.iac.es/Astronomy/observing/manuals/

[10] http://www.gtc.iac.es/instruments/osiris/media/zeropoints.html

Table 2
Log Observations of Teraelectronvolt Sources and Teraelectronvolt Candidates Obtained at GTC

	Grism B			Grism R			
Object	$t_{\rm Exp}$ (s)	Date	Seeing	$t_{\rm Exp}$ (s)	Date	Seeing	r
BZB J0035+1515	2100	2015 Sep 30	0.6	1800	2015 Oct 01	0.6	17.00
1ES 0033+595	3600	2015 Sep 18	1.3	2700	2015 Sep 25	0.9	17.80
S2 0109+22	750	2015 Sep 19	1.8	750	2015 Sep 19	1.8	15.20
RGB J0136+391	900	2015 Sep 28	0.9	600	2015 Sep 28	0.9	15.80
S3 0218+357	3600	2015 Feb 05	0.9	8700	2015 Feb 05	1.2	19.90
3C 66A	750	2015 Sep 09	0.8	210	2015 Sep 06	0.8	14.70
VER J0521+211	900	2015 Sep 21	0.8	1050	2015 Sep 21	0.8	16.40
1ES 0647+250	1500	2015 Sep 22	1.4	1200	2015 Sep 22	1.4	15.80
S5 0716+714	210	2015 Nov 30	1.6	210	2015 Nov 30	1.6	13.60
BZB J0915+2933	750	2015 Dec 24	2.0	450	2015 Jun 06	2.0	15.90
S4 J0954+65	300	2015 Feb 28	1.0	450	2015 Feb 28	1.0	15.5
BZB J1120+4212	3000	2016 Jun 24	1.5	3600	2015 Jul 01	0.7	16.10
1ES 1215+303	900	2015 May 20	1.5	900	2015 May 20	1.5	14.50
W Comae	1800	2015 Jun 30	1.4	1800	2015 Jun 30	1.4	15.50
MS 1221.8+2452	3000	2015 May 31	1.3	3000	2015 May 31	1.2	16.70
S3 1227+255	450	2015 Dec 25	1.5	500	2015 Dec 25	1.5	14.90
BZB J1243+3627	1350	2015 May 21	1.2	1350	2015 May 21	1.2	15.60
BZB J1248+5820	600	2015 Dec 25	2.2	900	2015 Dec 25	2.2	15.70
PKS 1424+240	450	2015 Jun 30	1.0	450	2015 Jun 30	1.0	14.20
BZB J1540+8155	900	2015 Jun 23	1.0	900	2015 Jun 23	1.0	17.30
RGB J2243+203	600	2015 Sep 19	2.0	750	2015 Sep 19	2.0	16.20
BZB J2323+4210	3000	2016 Aug 07	1.3	3600	2015 Feb 28	0.7	17.50

Note. Col. 1: Name of the target; Col. 2: Total integration time with Grism B; Col. 3: Date of observation with Grism B; Col. 4: Seeing during the observation with Grism B; Col 5: Total integration time with Grism R; Col. 6: Date of observation with Grism R; Col. 7: Seeing during the observation with Grism R; Col. 8: r' mag measured on the acquisition images.

Table 3
Properties of the Optical Spectra of Observed Sources

OBJECT	α	S/N	$\rm EW_{min}$	$z_{\rm lim}$	z	$N/H_{\rm lim}$
BZB J0035+1515	−1.3	183–275	0.09–0.18	0.55 (0.32)	⋯	11
1ES 0033+595	*	40–135	0.27–0.52	0.53 (0.10)	0.467[e]	5
S2 0109+22	−1.0	167–375	0.07–0.16	0.35 (0.15)	⋯	20
RGB J0136+391	−1.5	196–482	0.08–0.15	0.27 (0.14)	⋯	6
S3 0218+357	*	5–20	*	*	0.944[e]	3
3C 66A	−1.1	118–314	0.10–0.22	0.10 (*)	⋯	2
VER J0521+211	−0.9	82–221	0.15–0.37	0.18 (0.10)	⋯	1
1ES 0647+250	−1.3	115–294	0.09–0.21	0.29 (0.12)	⋯	7
S5 0716+714	−0.8	180–346	0.04–0.14	0.10 (*)	⋯	4
BZB J0915+2933	−1.1	89–241	0.14–0.34	0.13 (*)	⋯	1
S4 J0954+65	−0.9	50–120	0.15–0.20	0.45 (0.27)	⋯	25
BZB J1120+4212	−1.6	100–190	0.12–0.23	0.28 (0.12)	⋯	5
1ES 1215+303	−1.0	205–375	0.09–0.14	0.14 (*)	0.129[e]	4
W Comae	−0.6	180–260	0.09–0.17	0.19 (0.10)	0.102[e,g]	1
MS 1221.8+2452	−1.2	115–199	0.13–0.23	0.34 (0.15)	0.218[e,g]	2
S3 1227+25	−0.8	124–397	0.09–0.24	0.10 (*)	⋯	2
BZB J1243+3627	−1.3	208–465	0.05–0.15	0.28 (0.10)	>0.48[a]	29
BZB J1248+5820	−0.9	76–225	0.12–0.29	0.14 (*)	⋯	2
PKS 1424+240	−1.1	254–436	0.04–0.10	0.10 (*)	0.604[e]	184
BZB J1540+8155	−1.3	97–211	0.15–0.28	0.56 (0.22)	>0.67[a]	14
RGB J2243+203	−1.1	109–178	0.15–0.22	0.22 (0.10)	⋯	3
BZB J2323+4210	−1.2	160–315	0.07–0.17	0.73 (0.65)	>0.267[a]	1

Note. Col. 1: Name of the target; Col. 2: Optical spectral index derived from a power-law fit in the range 4250–10000; Col. 3: range of S/N of the spectrum; Col. 4: Range of the minimum equivalent width ($\rm EW_{min}$) derived from different regions of the spectrum (see text); Col. 5: Lower limit (3σ level) of the redshift by assuming a BL Lac host galaxy with $M_R = -22.9$ (−21.9). In parentheses we give the redshift lower limit assuming a host galaxy one magnitude fainter. An asterisk indicates that the redshift limit is out of the observed range for the case of a fainter host galaxy (see the Appendix); Col. 6: Spectroscopic redshift; the superscript letters are e = emission line, g = host galaxy absorption, a = intervening absorption; Col. 7: Lower limit of the nucleus-host galaxy ratio (N/H) in the r band considering the whole flux of the host galaxy.

were then calibrated to have the flux at 6231 Å equal to the photometry found for the targets (see Table 2). Finally, each spectrum has been dereddened, applying the extinction law described in Cardelli et al. (1989) and assuming the $E(B-V)$ values taken from the NASA/IPAC Infrared Science Archive.[11]

4. Results

The optical spectra of the targets are presented in Figure 4. In order to emphasize weak emission or absorption features, we also show the normalized spectrum. This was obtained by dividing the observed calibrated spectrum by a power-law continuum fit of the spectrum, excluding the telluric absorption bands (see Table 3). These normalized spectra were used to evaluate the signal-to-noise ratio (S/N) in a number of spectral regions. On average, the S/N ranges from 150 to 200 at 4500 Å and 8000 Å, respectively, to a peak of 320 at 6200 Å. See details in Table 3, and all these spectra can be accessed at the website http://www.oapd.inaf.it/zbllac/

4.1. Search for Emission and Absorption Features

All spectra were carefully inspected to find emission and absorption features. When a possible feature was identified, we determined its reliability by checking that it was present on the three individual exposures (see Section 3 for details). We were able to detect spectral lines for nine targets. In particular, we observe [O III] 5007 Å weak emission in the spectra of 1ES 1215+303, W Comae, MS 1221.8+2452, and PKS 1424+240; [O II] 3727 Å in 1ES 0033+595, 1ES 1215+303, and PKS 1424+240; the Ca II 3934, 3968 Å doublet absorption system and the G-band 4305 Å absorption line in MS 1221.8+2452; a strong emission of Mg II 2800 Å in S3 0218+357 and intervening absorption systems due to Mg II 2800 Å in BZB J1243+3627 and BZB J1540+8155; and finally the Ca II 3934, 3968 Å doublet in the spectrum of BZB J2323+4210. Details are found in Figure 5 and Table 5. The spectra of seven additional targets are found to be completely featureless, even though a redshift is reported in the literature. Details about the optical spectra and redshift estimates for each object in our sample are given in Section 5.

4.2. Redshift Lower Limits

Based on the assumption that all BLLs are hosted by a massive elliptical galaxy (e.g., Falomo et al. 2014), one should be able to detect faint absorption features from the starlight provided that the S/N and the spectral resolution are sufficiently high. In the case of no detection of spectral features, it is possible to set a lower limit to the redshift based on the minimum equivalent width (EW) that can be measured in the spectrum.

The minimum measurable equivalent width (EW_{min}) was set according to the scheme outlined by Sbarufatti et al. (2006a, 2006b), though in a more elaborated procedure (see Appendix). In brief, from the normalized spectrum (see Figure 4), we computed the nominal EW by adopting a running window of 15 Å for five intervals of the spectra that avoid the prominent telluric absorption features (see Table 3). The procedure yields for each given interval a distribution of EW, and we took 3 times the standard deviation of the distribution as the minimum measurable EW (see details in the Appendix).

[11] https://irsa.ipac.caltech.edu/applications/DUST/

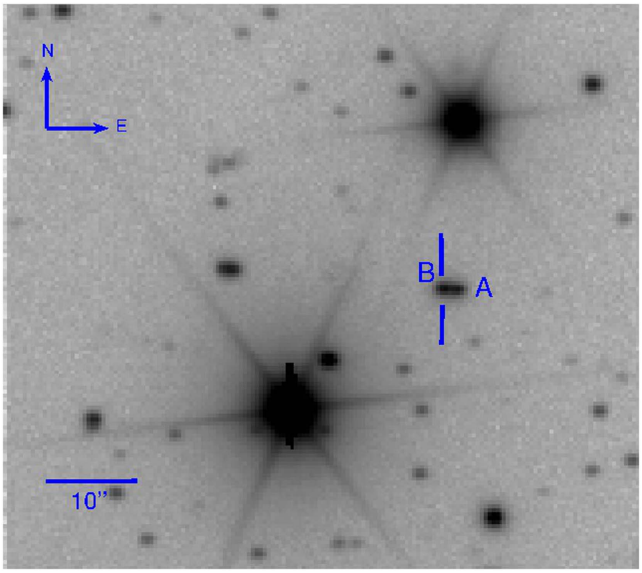

Figure 1. The *r*-band optical image of the sky region around the BL Lac object 1ES 0033+595 obtained at the GTC. The source flagged as "A" is a foreground star, and the BLL is the source labeled as "B."

Five different intervals were considered because the S/N changes with wavelength. The range of EW_{min} is reported in Table 3, and we give a lower limit on z assuming a standard average luminosity for the host galaxy $M_R = -22.9$ (or $M_R = -21.9$ in parentheses).

5. Notes for Individual Sources

BZB J0035+1515: The source was first discovered by Fischer et al. (1998) and cataloged as a BLL on the basis of its featureless optical spectrum. A more recent optical spectrum, obtained as part of the SDSS survey, exhibits no features (although the automatic procedure suggests some tentative values, also included in the NASA/IPAC Extragalactic Database; NED). Also Shaw et al. (2013) found a featureless spectrum.

We confirm the featureless nature of the spectrum from 4200 to 9000 Å, and from our high S/N we obtain an EW_{min} of 0.09–0.18 Å, which corresponds to a redshift lower limit of $z > 0.55$.

1ES 0033+595: Perlman et al. (1996) identified this Einstein Slew Survey source as a BLL, finding a featureless optical spectrum (although a tentative redshift of $z = 0.086$ was derived by Perlman et al., as mentioned in Falomo & Kotilainen 1999). In Scarpa et al. (1999), the *HST* images of this object show two unresolved sources, "A" and "B," separated by 1.″58 and with magnitude $m_R = 17.95 \pm 0.05$ and 18.30 ± 0.05 mag, respectively. On the basis of radio coordinates, the authors identified the source B as the most probable BLL counterpart and A as a possible star.

In our spectrum, the two sources are partially resolved (see Figure 1), and we perform a deblending during the extraction process in order to obtain two separated spectra for the targets. The spectrum of the object "A" (Figure 2) shows the typical stellar absorption lines of G stars, confirming the previous classification. For the "B" source we obtain a spectrum with an S/N ∼ 100 (see Figure 4), and although there is some contamination of the spectrum by the companion, the nondetection of H_α indicates that the "B"

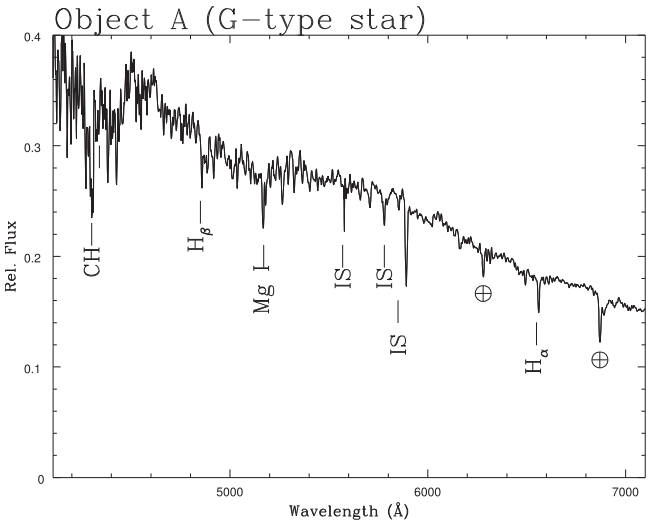

Figure 2. GTC spectrum of the companion source, labeled as "A" (see Figure 1), of the BL Lac object 1ES 0033+595. Absorption lines due to CH (4299 Å), hydrogen (4342, 4863, 6565 Å), and Mg I (5176 Å) are clearly detected. Telluric bands are indicated by ⊕. This object can be classified as a G-type star.

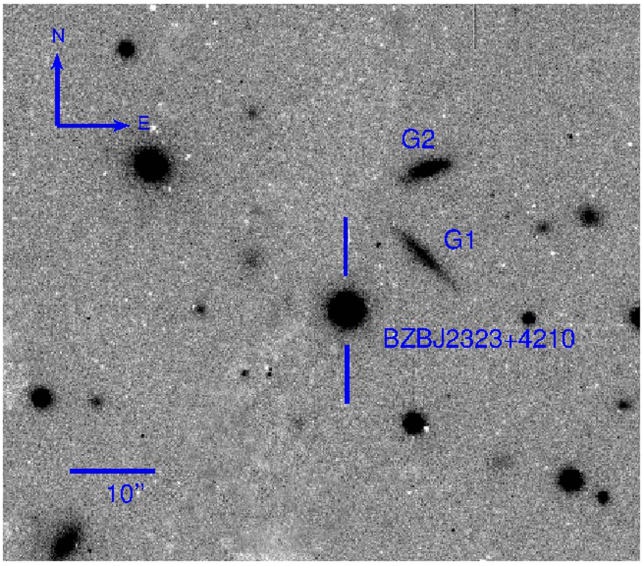

Figure 3. Optical R image of the BL Lac object BZB J2323+4210 taken at the NOT telescope (Falomo & Kotilainen 1999). Two spiral galaxies, labeled as G1 and G2, are present in the field of view of the BL Lac object at a distance of $\sim 8\farcs5$ and $\sim 12\farcs0$, respectively.

object has an extragalactic nature, and it is the blazar counterpart as proposed by Scarpa et al. (1999). We found an emission feature at 5468 Å of EW = 0.4 Å (see Figure 5). This feature is detected in all three individual spectra, and therefore we consider it a secure detection. If identified as [O II] 3727 Å emission, a tentative redshift of $z = 0.467$ can be provided.

Finally, comparing our photometry with Scarpa et al. (1999), we obtain the same value for the A object, while for the object B we obtain a magnitude difference of 1.2 with respect to the previous one, reinforcing the classification of this source as a BLL.

RGB J0136+391: The first identification of this source as a BLL was proposed by Laurent-Muehleisen et al. (1998), showing a featureless optical spectrum. The same result was found in Wei et al. (1999), Piranomonte et al. (2007), and Shaw et al. (2013). A lower limit on the redshift of $z > 0.40$ was set on the basis of high-quality *i*-band images obtained at the Nordic Optical Telescope (NOT; Nilsson et al. 2012).

We found our high S/N (∼200–480) optical spectrum completely featureless, only allowing us to set a lower limit to the redshift of $z > 0.27$.

S3 0218+357: This source was discovered to be a gravitational lens by Patnaik et al. (1993), who detected two similar radio sources with $\sim 0\farcs33$ separation and an Einstein ring with the same diameter. Optical counterparts of the two radio sources were observed and detected by *HST* images (Jackson et al. 2000; York et al. 2005). An optical spectrum of the source was obtained by Browne et al. (1993), who detected absorption features of Ca II and Mg II attributed to the lens galaxy at $z = 0.684$. They also claimed the detection of very weak emission lines of [O II] 3727 Å and [O III] 5007 Å. In addition, they suggested the presence of a weak emission feature of Mg II 2800 Å attributed to the blazar and proposed a redshift of 0.936. The redshift of the lens galaxy was confirmed through 21 cm H I absorption by Carilli et al. (1993). Cohen et al. (2003) obtained a high-quality spectrum that confirms the absorption features and clearly detected a strong, broad emission line at 5470 Å identified as Mg II 2800 Å, yielding a redshift of $z = 0.944$ for the blazar. In addition, these authors claimed the detection of emission lines of [O II], H_β, and [O III] at $z = 0.684$, attributed to the lens galaxy. Moreover, they claimed the detection of weak H_β and [O III] emission in the red noisy spectrum, also attributed to the blazar at $z = 0.944$.

We obtain an optical spectrum ranging from 4500 to 10000 Å with an S/N in the range 25–50. We confirm the detection of Mg II and Ca II absorption lines at $z = 0.684$, and in addition we clearly detect an absorption line at 9920 Å identified as Na I 5892 Å at the redshift of the lens. We do not detect the emission lines [O II], H_β, and [O III] (claimed by Cohen et al. 2003). We note that some of these latter features occur inside the telluric absorptions of O_2 and H_2O. We clearly detect the strong, broad emission line at 5480 Å (EW = 35 Å, FWHM = 4700 km s^{-1}) that, if attributed to Mg II 2800 Å, yields the redshift of $z = 0.954$. We stress that in our spectrum we do not detect the claimed emissions H_β and [O III] attributed to the blazar by Cohen et al. (2003). We note again that these features are placed in a spectral region that is heavily contaminated by strong H_2O atmospheric absorption. Therefore we conclude that the redshift of S3 0218+357 is still tentative since it is based on only one line. If confirmed, this source is the most distant blazar detected at frequencies >100 GeV (Ahnen et al. 2016).

It is worth noting that the shape of the continuum exhibits a marked decline toward the blue region that is rather unusual for this type of source. This could be due to significant intrinsic extinction or is caused by absorption in the lens.

3C 66A: Wills & Wills (1974) identified this strong radio source as a BLL because of its featureless optical spectrum. Miller et al. (1978) proposed a redshift of $z = 0.444$, on the basis of one emission line attributed to Mg II 2800 Å. This value was considered by the authors as tentative and

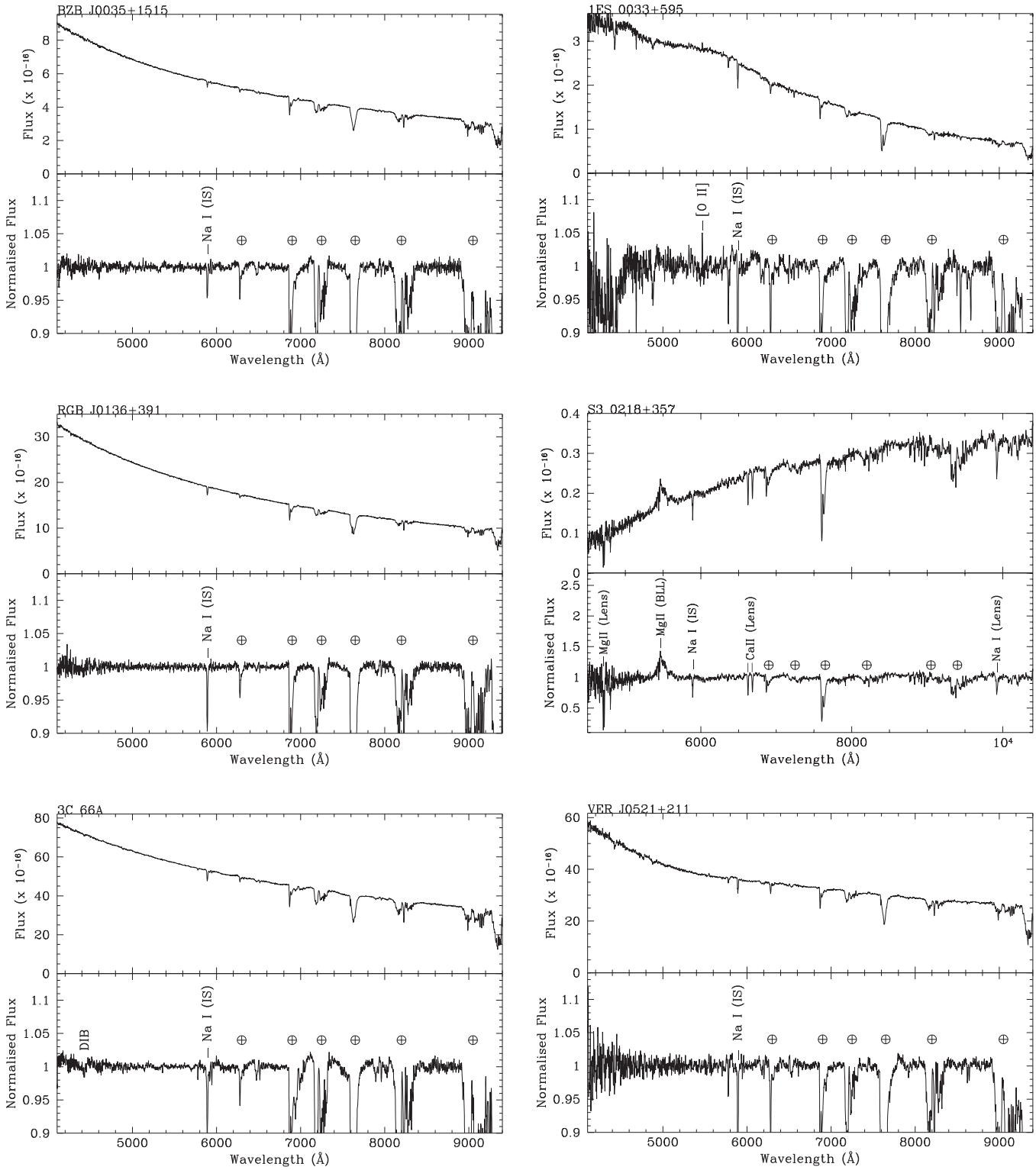

Figure 4. Spectra of the teraelectronvolt sources and teraelectronvolt candidates obtained at GTC. Top panel: flux-calibrated and dereddened spectra. Bottom panel: normalized spectra. The main telluric bands are indicated by ⊕, and the absorption features from the interstellar medium of our galaxies are labeled as IS (interstellar).

highly uncertain. No other optical spectroscopy was done for thirty years. More recently, Finke et al. (2008) showed an optical spectrum in the range from 4200 to 8500 Å with no detectable optical features. The featureless spectrum was also confirmed by Shaw et al. (2013).

Our high S/N (∼200) GTC spectrum is also featureless. Based on our procedure of redshift lower limits being estimated by EW_{min}, due to the relatively bright source we can set only a modest lower limit of $z > 0.10$. We are not able to confirm the Mg II emission proposed by Miller et al. (1978) because it is out

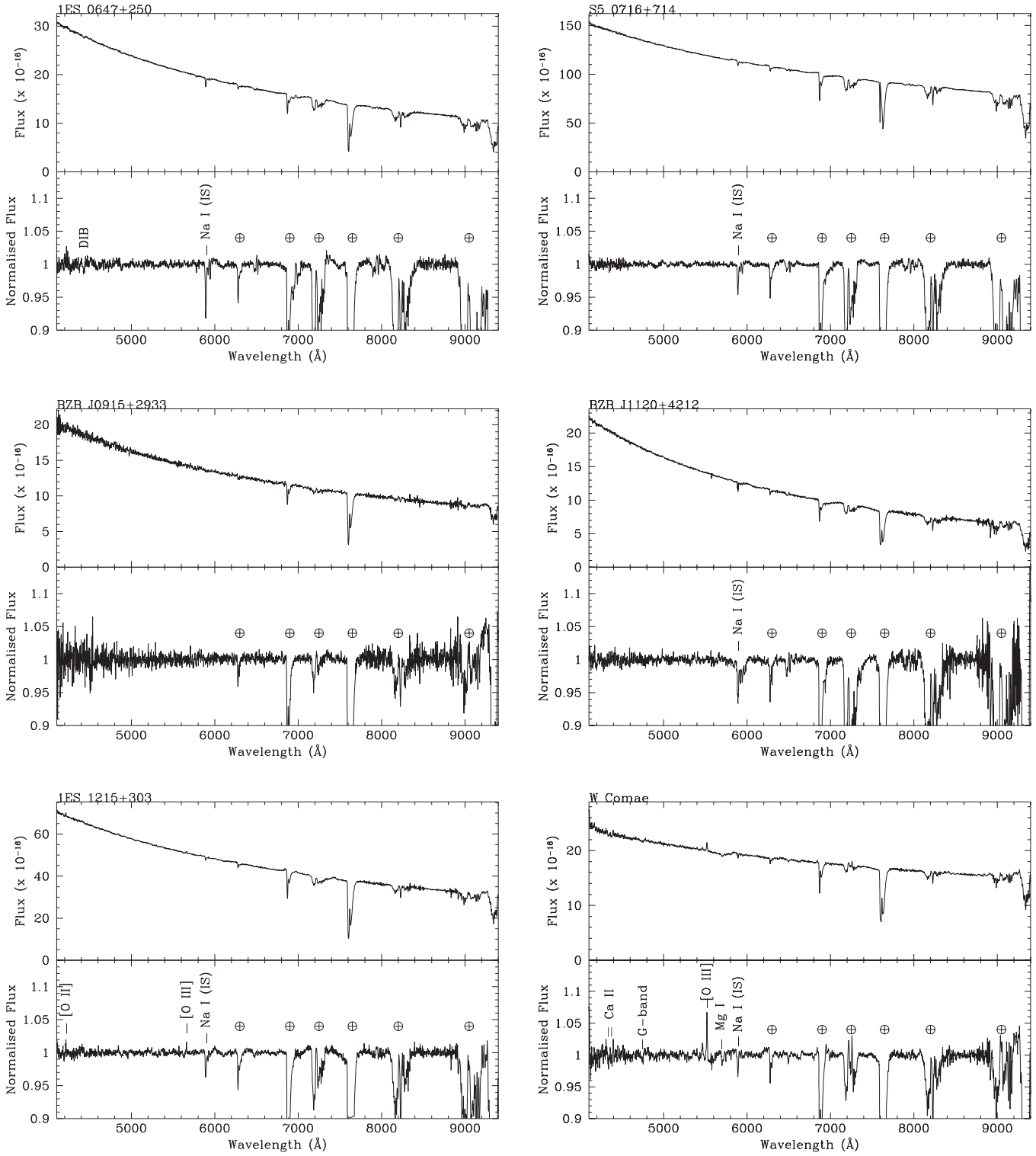

Figure 4. (Continued.)

of our spectral range. However, at $z = 0.444$ we would expect to observe the H_β emission line at 7020 Å, where we do not detect any line with EW > 0.2 Å. We conclude that the redshift of this source is still unknown.

VER J0521+211: On the basis of a weak emission line at 5940 Å attributed to [N II] 6583 Å, Shaw et al. (2013) proposed this source to be at $z = 0.108$. This feature was not confirmed by Archambault et al. (2013), who report a featureless spectrum.

We do not confirm the redshift of the source, which therefore is still unknown, setting a lower limit of $z > 0.18$.

1ES 0647+250: An optical spectrum of this source with modest S/N was found to be featureless by Schachter et al. (1993), a result later confirmed by a better spectrum obtained

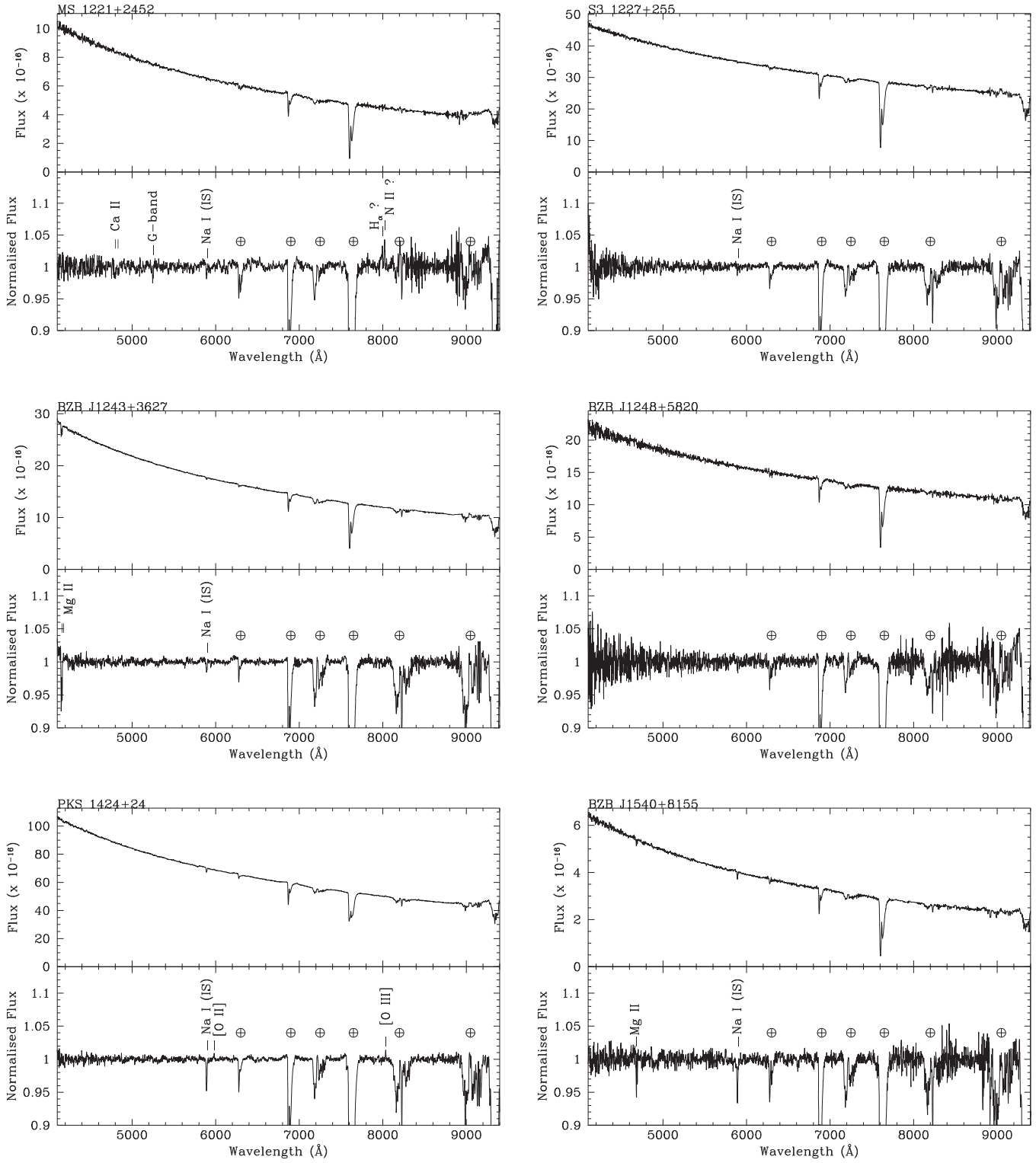

Figure 4. (Continued.)

with the Keck telescope by Shaw et al. (2013). A relatively high redshift can be supported by the absence of detection of the host galaxy from a high-quality image by Kotilainen et al. (2011).

Our GTC higher S/N (∼200) spectrum confirms this featureless behavior with absorptions at around 4400 Å and 4880 Å due to diffuse interstellar bands and at ∼6500 Å due to water vapor. On the basis of our spectrum, we set a lower limit of $z > 0.29$.

S5 0716+714: This is a bright ($V \sim 15$) and highly variable (Bach et al. 2007) source for which several attempts to detect the redshift failed (Stickel & Kuhr 1993; Rector & Stocke 2001; Finke et al. 2008; Shaw et al. 2013). From optical images, Sbarufatti et al. (2005a) set a lower limit of

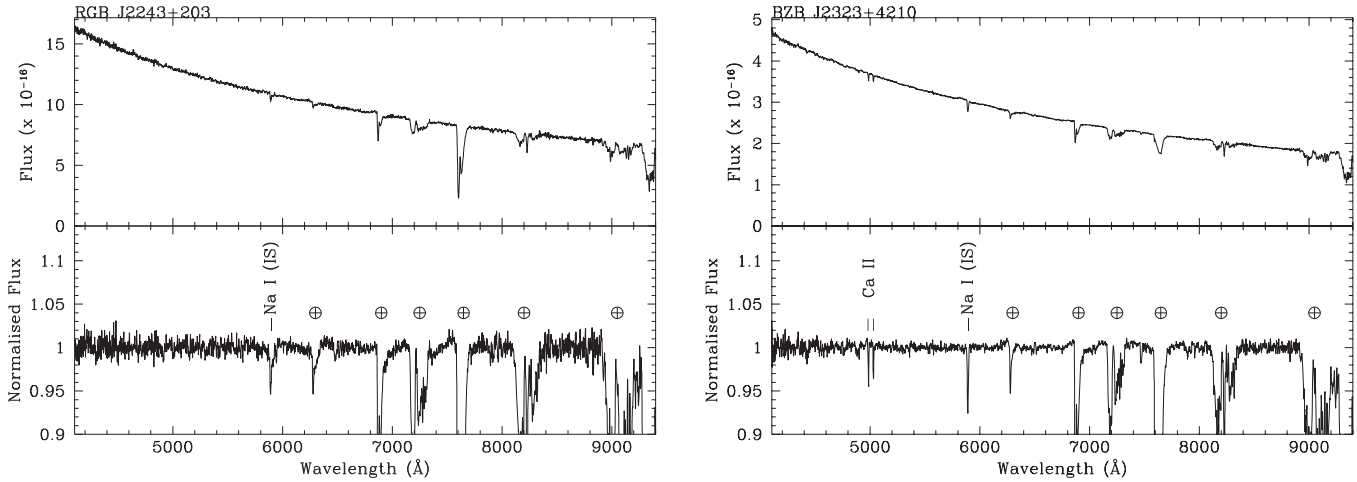

Figure 4. (Continued.)

$z > 0.5$, and Nilsson et al. (2008) provided an imaging redshift of $z \sim 0.3$ based on the marginal detection of the host galaxy. Finally, we note that Danforth et al. (2013), based on the distribution of the absorption systems, set a statistical upper limit of $z \lesssim 0.3$.

We obtained a featureless optical spectrum during a high state of the source ($r = 13.6$), and we can set a redshift lower limit of $z > 0.10$.

BZB J0915+2933: Wills & Wills (1976) showed a continuous optical spectrum for the source and classified it as a BLL. The featureless behavior was also found by White et al. (2000) and by Shaw et al. (2013).

Through our high S/N optical spectrum, we confirm the featureless spectrum and set a lower limit to the redshift of $z > 0.13$.

BZB J1120+4212: This object (also known as RBS 0970) is a point-like radio source detected by various X-ray surveys (see, e.g., Giommi et al. 2005). Optical spectral classification of the source as BLL was proposed by Perlman et al. (1996) on the basis of the quasi-featureless spectrum. They claim the detection of starlight absorption features at $z = 0.124$. However, based on the spectrum reproduced in their Figure 4, the reliability of this feature is quite uncertain. This redshift is not confirmed in other spectra obtained by White et al. (2000) and Massaro et al. (2014). Also, the spectrum obtained by SDSS (J112048.06+421212.4) appears to us to be featureless.

Our spectrum with S/N ∼ 100–190 is featureless, and we set a lower limit of $z > 0.28$.

1ES 1215+303: Bade et al. (1998) reported a redshift of $z = 0.130$ for this target, but no information about the detected lines is given. On the contrary, White et al. (2000) showed an optical spectrum claiming a redshift of 0.237, although it appears featureless from their figure.

A more recent spectrum (S/N = 60) obtained by Ricci et al. (2015) was also found to be featureless. The target was clearly resolved in *HST* exposures (Scarpa et al. 2000), revealing a massive elliptical host galaxy, suggesting the source is at low redshift.

Given these different redshift values, we secured a high-quality optical spectrum (S/N ∼ 300) in which we detect two emission lines: [O II] 3727 Å and [O III] 5007 Å at $z = 0.131$ (see also Table 5), confirming the low redshift previously reported.

W Comae: Weistrop et al. (1985) provided an optical spectrum and estimated a redshift of $z = 0.102$ based on the detection of [O III] 5007 Å and H_α emission lines. This redshift was not confirmed by Finke et al. (2008), though their spectra cover only the range from 3800 to 5000 Å. In addition, the spectrum obtained by the SDSS (J122131.69 +281358.4) proposes a redshift of $z = 1.26$. In 2003, the host galaxy of W Comae was resolved by Nilsson et al. (2003).

From our (S/N ∼ 220) optical spectrum, we confirm the detection of [O III] 5007 Å and H_α emission lines at $z = 0.102$. In addition, we detect at the same redshift the absorption lines due to the Ca II (3934, 3968 Å) doublet, the G-band 4305 Å, and Mg I 5175 Å from the host galaxy.

MS 1221.8+2452: A tentative redshift of $z = 0.218$ was proposed by Morris et al. (1991) and Rector et al. (2000). Imaging studies of this source were able to resolve the host galaxy and are consistent with the low redshift of the target (Falomo & Kotilainen 1999; Scarpa et al. 2000).

We detect the Ca II doublet and G-band 4305 Å absorption lines at $z = 0.218$, and we find emission lines at ∼7995 and ∼8020 *AA* that if confirmed could be attributed to H_α and N II 6583 Å.

S3 1227+255: Nass et al. (1996) reported $z = 0.135$, but no information on the detected spectral lines was provided. In spite of the alleged low redshift, high-quality images failed to detect the host galaxy (Nilsson et al. 2003). Shaw et al. (2013) did not confirm this redshift, and no spectral features were found.

Our optical spectrum (S/N ∼ 250) is featureless down to EW = 0.1–0.2 Å. Therefore we do not confirm the literature redshift, and we set a redshift lower limit of $z > 0.10$.

BZB J1243+3627: White et al. (2000) reported a featureless spectrum for this source. An absorption feature of Mg II 2800 Å at $\lambda \sim 4160$ Å was detected in the SDSS spectrum, suggesting a redshift of $z \geqslant 0.485$ (Plotkin et al. 2010). This redshift limit appears to be consistent with the marginal detection of the host galaxy by Meisner & Romani (2010), who estimated $z \sim 0.50$.

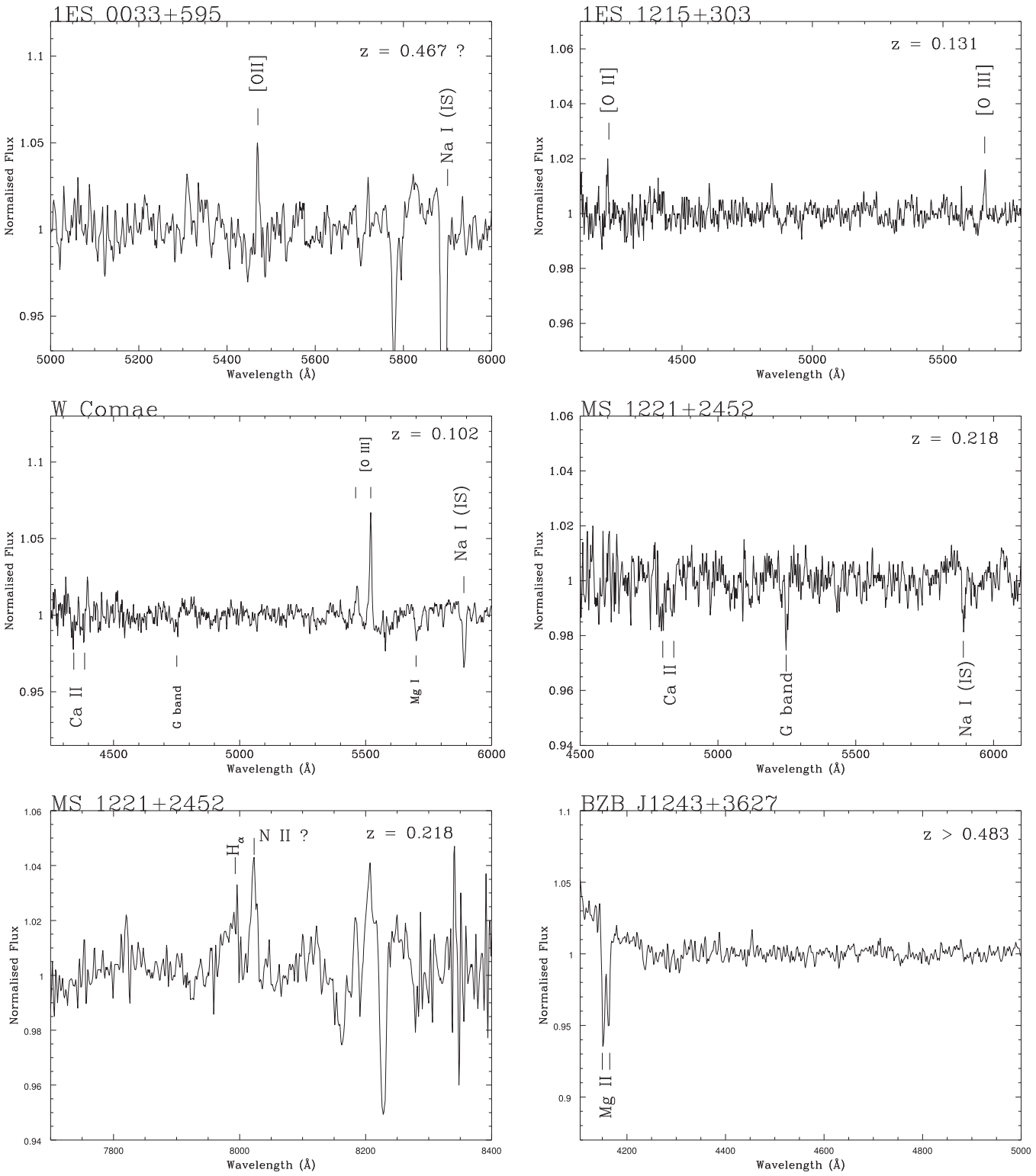

Figure 5. Close-up of the normalized spectra around the detected spectral features of the teraelectronvolt sources and teraelectronvolt candidates obtained at GTC. The main telluric bands are indicated by ⊕, and spectral lines are marked by line identification.

From our spectrum (S/N ∼ 330), we confirm the intervening absorption system due to Mg II 2800 Å, and the remaining part of the spectrum is completely featureless. The spectroscopic redshift lower limit is thus $z > 0.483$.

BZB J1248+5820: The source was classified as a BLL by Fleming et al. (1993), and no redshift was available. The featureless nature of the spectrum is reported in Henstock et al. (1997), Plotkin et al. (2008), and Shaw et al. (2013). Note that NED reports $z = 0.847$ based on the SDSS DR3 spectrum, although this is not confirmed by the SDSS DR13 analysis. Scarpa et al. (2000) failed to detect the host galaxy from *HST* images.

Our high S/N spectrum is featureless, and we can determine a lower limit to the redshift of $z > 0.14$.

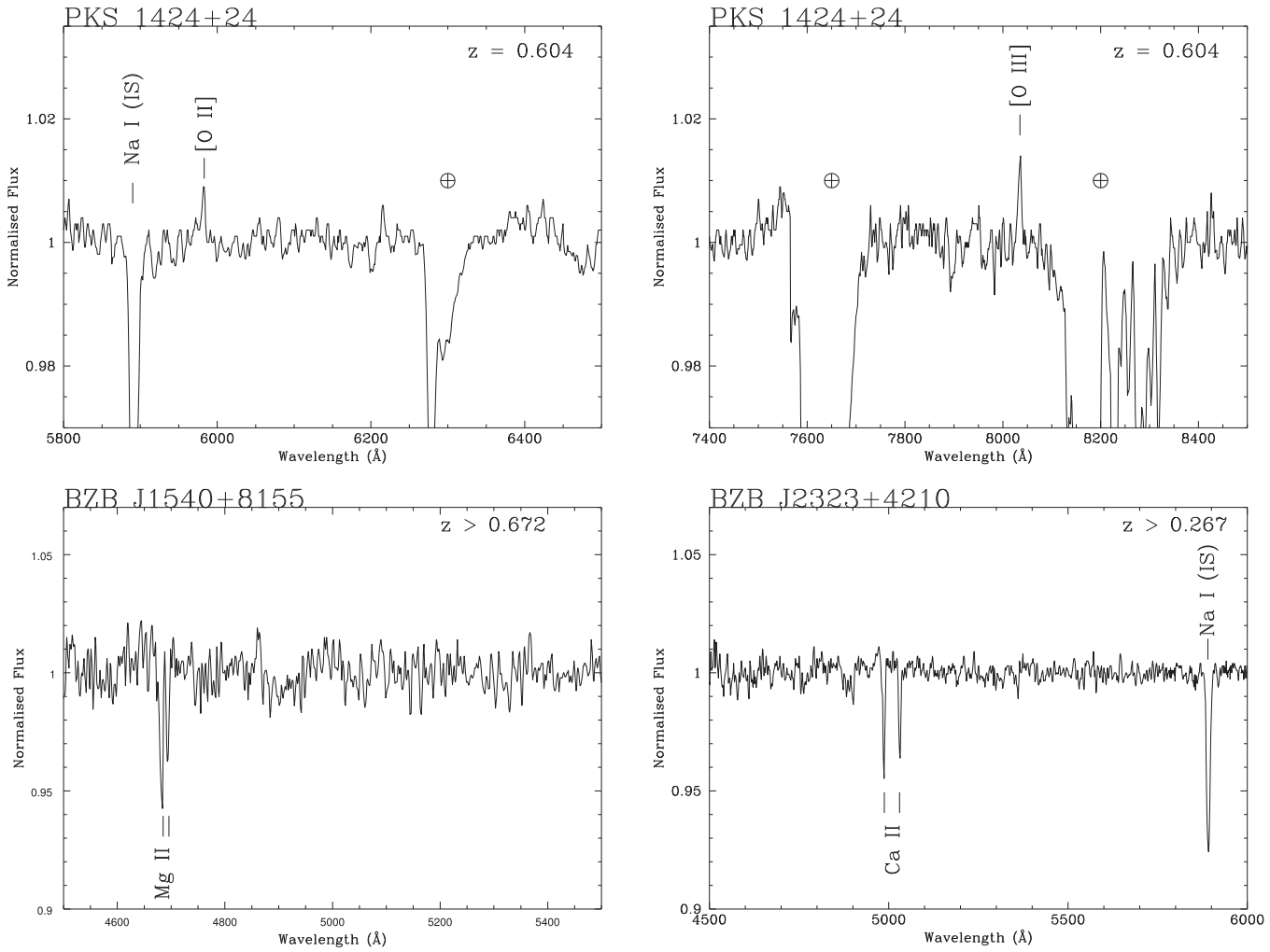

Figure 5. (Continued.)

PKS 1424+240: The source was classified as BLL by Fleming et al. (1993), and a featureless spectrum was reported by Marcha et al. (1996), White et al. (2000), and Shaw et al. (2013). Furniss et al. (2013), from the Ly$_\beta$ and Ly$_\gamma$ absorptions observed in the far-ultraviolet spectra from *HST*/COS (*Hubble Space Telescope*/Cosmic Origins Spectrograph) spectra, reported a lower limit of $z > 0.6035$. This is consistent with the nondetection of the host galaxy in *HST* images (Scarpa et al. 2000).

In our high S/N $\sim$ 350 optical spectrum, we detect two faint emission lines at 5981 and 8034 Å (see Figure 5), due to [O II] 3727 Å and [O III] 5007 Å. The redshift corresponding to this identification is 0.6047, suggesting that the absorber at that redshift limit is associated with the BLL. Note also that in the environment of the target there is a group of galaxies at $z \sim 0.60$, suggesting it is associated with the BLL (Rovero et al. 2016).

BZB J1540+8155: The source was identified as BLL by Schachter et al. (1993). The optical spectra obtained by Perlman et al. (1996) failed to detect emission or absorption features. The host galaxy was not detected by *HST* images (Scarpa et al. 2000), putting the source at relatively high redshift.

In our GTC spectrum, we detect an intervening absorption doublet at $\sim$4680 Å that we identify as Mg II 2800 Å absorption, yielding a spectroscopic redshift lower limit of $z > 0.673$. No intrinsic emission or absorption lines are found. The spectroscopic redshift limit is consistent with our redshift limits determined by the absence of detection of host-galaxy features.

RGB J2243+203: Laurent-Muehleisen et al. (1998) presented the first optical spectrum of this source, found to be featureless. Similarly, the spectrum obtained by Shaw et al. (2013) is featureless, but the authors claimed the detection of an absorption line at $\sim$3900 Å identified as Mg II (2800 Å). If confirmed, this would imply a redshift of $z > 0.395$.

Our spectrum, which does not cover the 3900 Å region, is very featureless from 4100 to 9000 Å with the limits on the emission or absorption lines of $\mathrm{EW_{min}} < 0.2$. This corresponds to a lower limit of $z > 0.22$.

BZB J2323+4210: From a poor optical spectrum, Perlman et al. (1996) claimed the detection of two starlight absorption features identified as Mg I (5175 Å) and Na I (5892 Å), and they proposed a redshift of $z = 0.059$. We disprove this redshift because the Na I absorption coincides with the telluric absorption at 6280 Å. Shaw et al. (2013) does not confirm this redshift either.

Our high S/N ($\sim$200) spectrum is characterized by a power-law emission ($F_\lambda \propto \lambda^\alpha$; $\alpha = -1.2$). We clearly detect

an absorption doublet at ∼5000 Å (EW ∼ 0.25 Å) and an absorption line at 7465 Å. We identify these features as Ca II 3934, 3968 Å, and Na I 5892 Å absorption lines at $z = 0.267$. If these lines were ascribed to the starlight of the host galaxy, we would expect to observe some modulation imprinted on the continuum, which is not present. Moreover, this redshift appears remarkably inconsistent with the lower limits ($z_{\rm lim} > 0.65$) derived from the nondetection of the host galaxy.

We further note these absorption features are rather narrow (FWHM ∼ 10 Å) compared to the typical Ca II line width from galaxies and are indicative of interstellar absorptions. Indeed, at ∼8.″5 and 12″ (southeast) from the target (see Figure 3), there are two spiral galaxies with halo gas that could be responsible for the absorption features observed. At $z = 0.267$, the projected separation between the target and these galaxies is ∼40 kpc.

We conclude that the redshift of BZB J2323+4210 is still unknown, and we set a spectroscopic lower limit of $z > 0.267$ and a lower limit based on the host-galaxy feature of $z > 0.65$ (see also Archambault et al. 2016).

The case has some analogy with that of the BLL MH 2136-428 (Landoni et al. 2014), where narrow absorption lines appear in the spectrum due to the halo of an interloping bright galaxy.

6. Discussion

We secured high S/N spectra in the range 4200–9500 Å for a sample of 22 BLLs, selected for being TeV emitters or good candidates based on their IR properties. Most of these sources either had an unknown redshift or the value was rather uncertain. From the new spectroscopy we are able to determine the redshift for five objects (S3 0218+357, 1ES 1215+303, W Comae, MS 1221.8+2452, and PKS 1424+240). For PKS 1424+240, one of the farthest BLLs detected in the TeV regime, no previous estimate of the redshift was available. For three objects, BZB J1243+3627 with an uncertain redshift and BZB J1540+8155 and BZB J2323+4210 with previously unknown redshift, we found intervening absorptions that allow us to set spectroscopic lower limits. For the remaining 13 sources, we found that in spite of the high S/N their spectrum is featureless. We can set limits to any emission or absorption features to 0.05–0.50 Å depending on the S/N of the targets and the wavelength region. For seven of these targets, there was a previous tentative redshift that we do not confirm from our observations. The main reasons for this difference are as follows: old spectra have poor S/N, wrong source identification, very tentative line identifications, and redshift given without information on the detected spectral features (no spectrum shown). It is worth noting that unfortunately these unconfirmed, likely wrong values (also appearing in NED) are often used to derive physical properties of the sources.

On the basis of the assumption that all of the objects with pure featureless spectra are hosted by a massive elliptical galaxy, as is the case for most (virtually all) BLLs, we have then determined a lower limit for their redshift from the minimum detectable EW of some absorption lines of the host galaxy (see the Appendix for details). Depending on the brightness of the observed nuclei ($r = 13.6$–19.9), we can set redshift lower limits for these objects from $z = 0.1$ to $z = 0.55$ (see Table 3).

In addition to the lower limits of the redshift for objects with featureless spectra, we can also estimate an average upper limit for the redshift of the sample of observed targets based on the number of Mg II 2800 Å intervening absorption systems observed in our spectra. Given our observed spectral range, we are potentially able to detect Mg II 2800 Å intervening absorption lines (of EW $\gtrsim 0.2$ Å) for absorbers that are at $z > 0.5$. Excluding the objects that are at $z < 0.5$ (four sources), we observe two absorption systems of Mg II over 18 targets. To evaluate an average upper limit to the redshift of these sources, we compute the expected number of Mg II intervening absorptions as a function of the redshift. To this aim, we assume the cumulative incidence rates of Mg II absorbers derived for a very extended sample of QSO spectra obtained by SDSS (Zhu & Ménard 2013). It turns out that the average maximum redshift of the sample is inferred to be $z \sim 0.65$. At higher redshift we would expect to detect many more absorption systems. For instance, if the average redshift of these sources were $z = 1$, we should detect ∼10 Mg II absorption systems in the spectra of 18 targets.

The relatively low upper limit of the redshift derived above together with the lack of detection of absorption lines from the host galaxies suggests that these targets have a high nucleus-to-host galaxy ratio. For each object with a featureless continuum, we have derived a lower limit to the redshift on the basis of the assumption that the source is hosted by a massive early-type galaxy (see the Appendix for details) and at a given limit of detectable EW of an absorption feature. We can now associate a minimum N/H to these redshift lower limits (see Table 3). It turns out that some objects in our sample have an $N/H > 10$ (assuming the targets are hosted by a "standard galaxy"; e.g., Falomo et al. 2014). This is significantly higher than the typical value ($N/H \sim 1$) for BLLs for which the host galaxy is directly imaged by *HST*, and it is similar to that estimated for unresolved sources at relatively high ($z = 0.5$–1.0) redshift (see, e.g., Urry et al. 2000). Since on average our targets are likely at moderate redshift (see above), the high N/H is suggestive of a particularly beamed nuclear emission. How strong could be the flux from the nucleus compared with that of its host galaxy? For an extremely high Doppler factor δ, we could have $N/H \sim 1000$. Detection of the spectral features of the host galaxy therefore will require observations with very high S/N and adequate spectral resolution. This appears feasible only in the Extremely Large Telescope (ELT) era (see e.g., Landoni et al. 2014).

Appendix
Redshift Lower Limit of BL Lac Objects from Host-galaxy Absorption Lines

Given the featureless nature of many BL Lac sources, it is of great interest to estimate lower limits of the redshift for these kind of targets and in particular for those that are also emitters (or candidates) at γ frequencies. In the cases where no spectral features are detected, the only way to estimate the redshift or a lower limit from optical data is to use the characteristics of the host galaxies. A direct method is to use high-quality images to detect the surrounding nebulosity, or to assess upper limits of the host brightness and then derive a redshift lower limit. Alternatively one can search for the host-galaxy features that

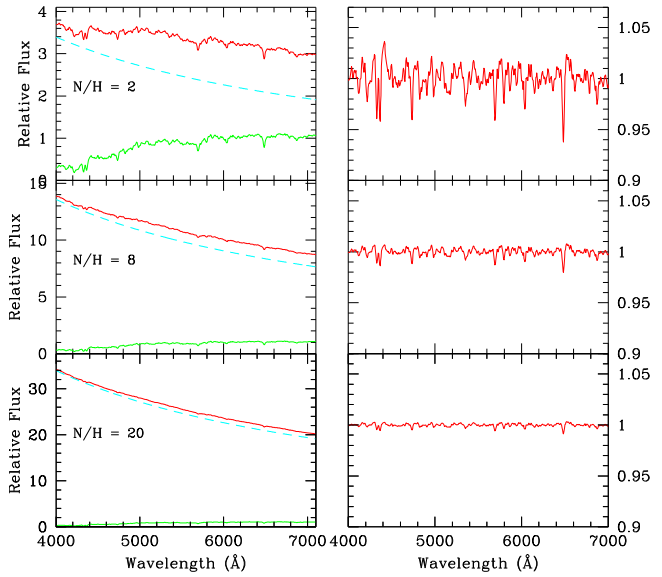

Figure 6. Left: simulation of the optical spectrum of a BL Lac object at $z = 0.2$ for different nucleus-to-host galaxy ratios. The values of N/H refer to the r band. The nonthermal component is assumed a power law with spectral index -1. No noise is included. Right: the normalized spectrum of the source (nonthermal plus starlight). The figure illustrates the effect of the nonthermal component to dilute the equivalent width of the spectral features.

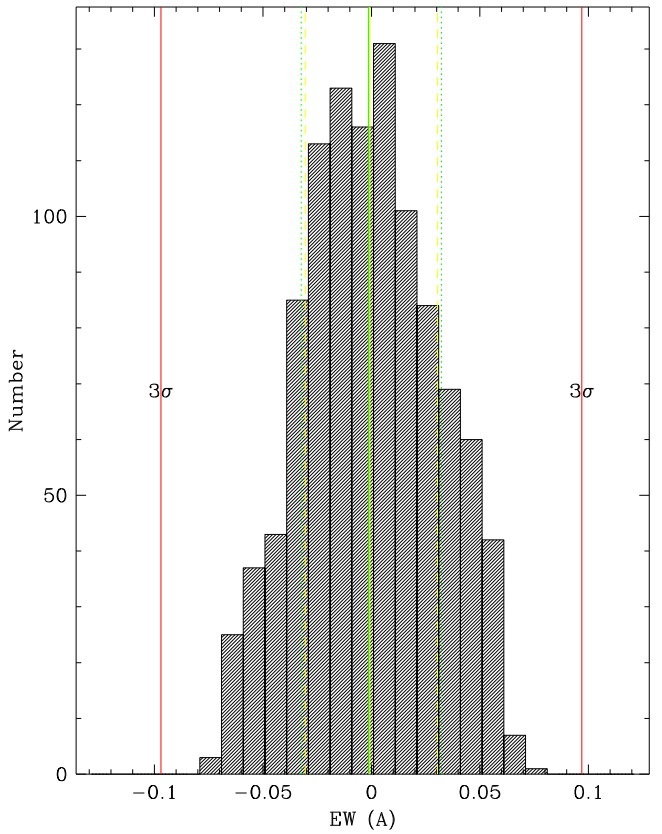

Figure 7. Distribution of all measurements of EW computed in a defined spectral interval (avoiding the telluric bands) by adopting a running window of fixed size. The EW_{min} is defined as 3 times σ_{EW} where σ_{EW} is the standard deviation of the distribution (see text for more details).

are heavily obscured by the dominant nonthermal emission (Sbarufatti et al. 2006a). In the first case, high-resolution and deep images are required, while in the second one, very high

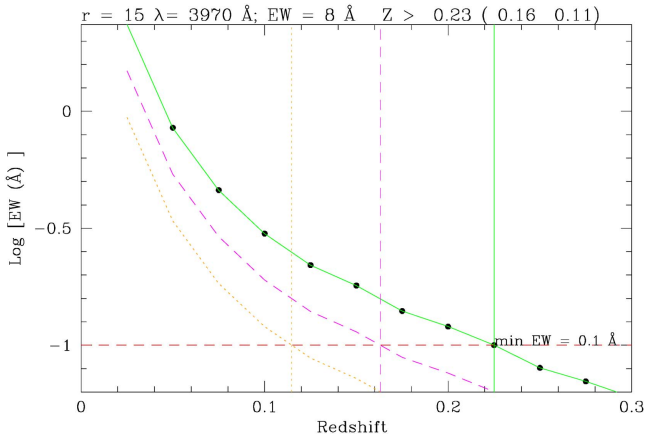

Figure 8. The relation between the EW of the Ca II absorption feature (assuming EW = 8 Å) and the redshift for the spectrum of a BL Lac object of magnitude $r = 15$. The relation assumes that the host galaxy has $M(R) = -22.9$ (green solid line and solid circles). The other two similar relations are for $M(R) = -22.4$ (magenta dashed line) and $M(R) = -21.9$ (orange dotted line). The dashed horizontal line gives the assumed EW_{min} level (0.1 Å), and the vertical lines represent the intersection with the above relationships with EW_{min} level. In this case the redshift is $z > 0.23$ (for the average host galaxy; other values in parentheses).

S/N spectra of adequate resolution are needed. Here we focus on this second approach.

Assuming the observed targets have giant elliptical host galaxies of similar luminosity distribution as the population of BLLs for which the host galaxy has been resolved, it is plausible to assume that they are hosted by massive early-type galaxies (see, e.g., Falomo et al. 2014 and references therein). Since the luminosity distribution of these host galaxies is relatively narrow (see, e.g., Urry et al. 2000), it is possible to use the host-galaxy luminosity as a sort of standard candle to evaluate the distance of the objects or to set lower limits in the cases where no signature from the starlight is found (Sbarufatti et al. 2006a).

In order to estimate lower limits for the redshift of lineless objects, we follow and extend the procedure proposed by Sbarufatti et al. (2006a) for good S/N optical spectra. The basic idea is that, under the assumption that the observed spectrum is due to the contribution of a (often dominant) nonthermal component, usually described by a power law, and to a starlight component from a *standard* host galaxy (see example Figure 6), it is possible to set lower limits on their redshift.

In fact, the effect of the strong nonthermal emission is to dilute the EW of the absorption features of the host galaxy depending on the flux ratio of the two components (nonthermal and starlight). Using high S/N spectra, it is thus possible to set suitable upper limits on the EW of the absorption features from the host galaxy. These limits depend on the S/N and the spectral resolution of the observations and on the brightness of the source.

We assume that the underlying host galaxy is a giant elliptical of absolute magnitude $M(R) = -22.9$ (Sbarufatti et al. 2005a) and use the spectrum template of Kinney et al. (1996).

For each observed spectrum, we then evaluate the dilution factor of an absorption line (namely H,K of Ca II 3924, 3970 Å, G-band 4304 Å, Mg I 5175 Å) of this host galaxy as a function

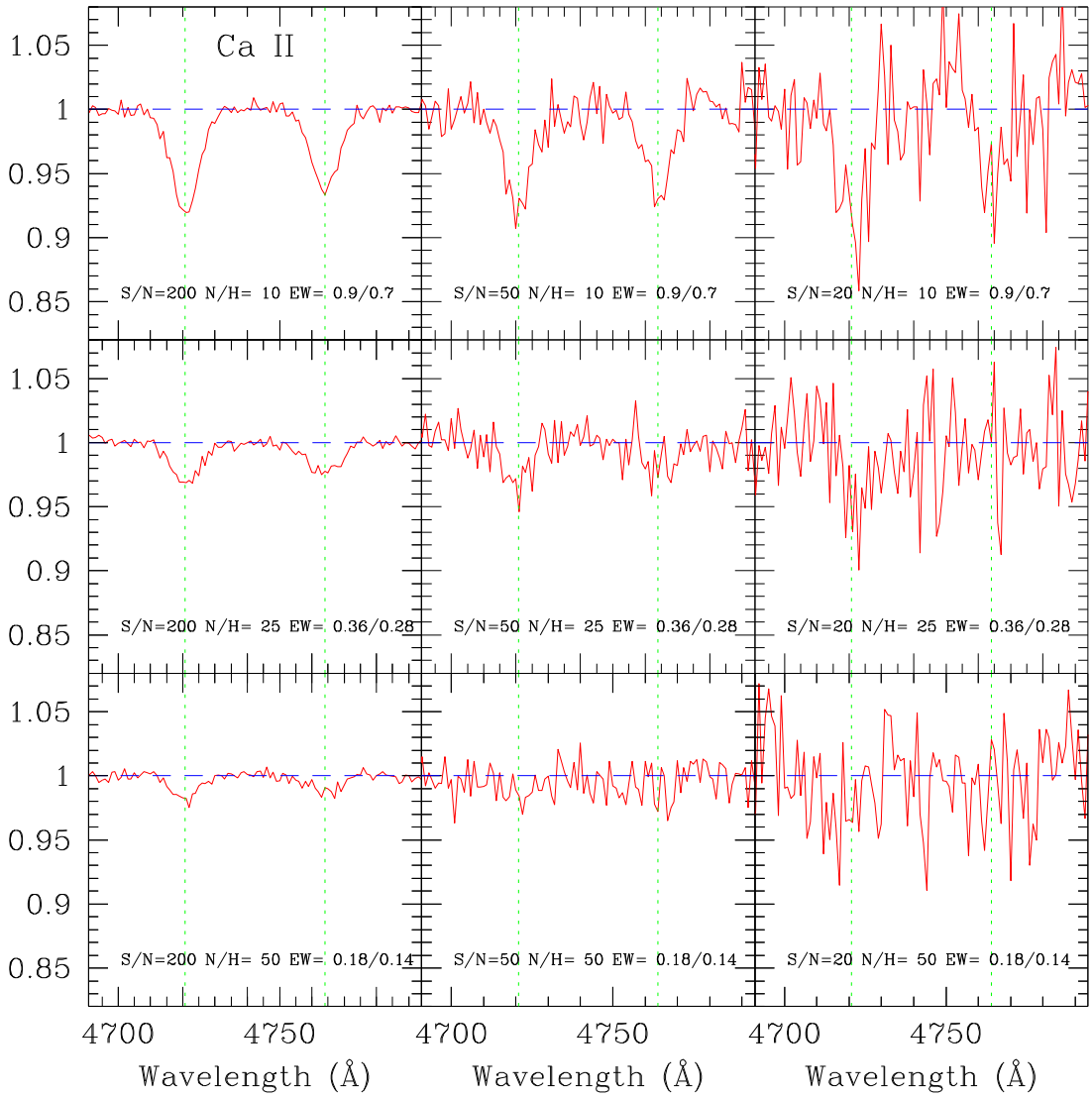

Figure 9. Simulation of the normalized optical spectrum of a BL Lac object at $z = 0.2$ in the region of the H, K Ca II lines. The simulation assumes three different nucleus-to-starlight flux ratios at the observed wavelength of the Ca II lines (from top to bottom) and three levels of S/N (from left to right). The two dotted vertical lines indicate the position of the H, K features for reference. The horizontal dashed line gives the normalized continuum. The simulation includes the statistical noise. The figure illustrates how the detectability of Ca II lines depends on N/H and S/N (see also text). In each panel we give the S/N of the spectrum, the nucleus-to-host ratio, and the minimum EW assuming standard or 1 mag fainter host-galaxy luminosity.

Table 4
Correspondence between the Wavelength Range, Absorption Lines, and Redshift Range

Wavelength Range	Absorption Line	Redshift Range
4250–5000	Ca II	0.08–0.27
5000–6200	Ca II	0.27–0.58
6400–6800	Ca II	0.63–0.73
7800–8100	Mg I	0.51–0.57
8400–8900	Mg I	0.63–0.72

Note. Col. 1: Wavelength range of the optical spectrum; Col. 2: Host galaxy absorption line used; Col. 3: Redshift range corresponding to the wavelength range.

of the redshift. To perform this, we took into account both k correction (using the host-galaxy template spectrum) and the starlight flux lost through the slit. The latter term was computed by assuming that the host galaxy has a de Vaucouleurs brightness profile and an effective radius Re = 8 kpc.

From the observed magnitude of the source and the assumption that the underlying host galaxy is a giant elliptical, we derive the minimum redshift of the target from the minimum detectable equivalent width (EW_{min}) of a specific absorption feature (see example in Figure 8). This depends on the S/N of the spectrum and the brightness of the object during the observations. To estimate EW_{min} we computed the nominal EW by adopting a running window of fixed size (typically 15 Å) for a number of intervals where the S/N is approximately constant and avoiding the prominent telluric absorption bands. For each interval, we define $EW_{min} = 3 \times \sigma_{EW}$ where σ_{EW} is the standard deviation of the distribution of all measurements of EW (see Figure 7). For each spectral interval, a given feature (for instance Ca II absorption) is considered detected only if the S/N is sufficiently high to measure the absorption feature with $EW > EW_{min}$. In Figure 9 we show an example of simulated optical spectra of BLLs in the region of

Table 5
Measurements of Spectral Lines

OBJECT	λ_{obs} Å	EW (Observed) Å	Line ID	z_{line}
1ES 0033+595	5468	0.40	[O II] 3727	0.467
S3 0218+357	5470	46.8	Mg II 2800	0.954
1ES 1215+303	4214	0.16	[O II] 3727	0.131
	5661	0.11	[O III] 5007	0.131
W Comae	4747	0.15	G-band 4305	0.102
	5520	0.65	[O III] 5007	0.102
	5704	0.30	Mg I 5175	0.102
	6496	0.31	Na I 5892	0.102
MS 1221.8+2452	4794	0.18	Ca II 3934	0.218
	4834	0.16	Ca II 3968	0.218
	5244	0.20	G-band 4305	0.218
	7995	0.35	H_α 6563	0.218
	8022	0.40	N II 6583	0.218
BZB J1243+3627	4150	0.90	Mg II 2800	>0.483
PKS 1424+240	5981	0.05	[O II] 3727	0.604
	8035	0.10	[O III] 5007	0.604
BZB J1540+8155	4680	0.60	Mg II 2800	>0.672
BZB J2323+4210	4987	0.30	Ca II 3934	>0.267
	5031	0.22	Ca II 3968	>0.267
	7470	0.35	Na I 5892	>0.267

Note. Col. 1: Name of the target; Col. 2: Barycenter of the detected line; Col. 3: Measured equivalent width; Col. 4: Line identification; Col. 5: Spectroscopic redshift.

Ca II absorption lines assuming different values for the N/H and S/N.

We used the EW_{min} of Ca II and MgI to derive lower limits for the redshift of featureless BLLs in our sample (see Table 3 and Table 4). These limits range from 0.1 to 0.55 Å. For a number of sources, other authors have derived redshift limits based on a similar approach but with somewhat different results. In particular, Shaw et al. (2013) propose redshift limits for 15 objects of our sample. For about one-half of them, the difference of the redshift limit is small and could be explained by some differences in the adopted method. Shaw et al. (2013) adopt the method proposed by Plotkin et al. (2010), who perform a best fit of the observed spectrum with a host-galaxy template and a power law and set a 2σ level threshold to assess the redshift (compared with 3σ assumed in our work). However, in some cases, Shaw et al. (2013) claim redshift limits that are significantly higher than those derived in this work. For instance, in the case of RGB J0136+391, we found $z > 0.27$, while Shaw et al. (2013) gives $z > 0.88$. The brightness level of the source was similar during the two observations, and also the S/N (estimated roughly only from the figures presented by Shaw et al.). We believe that the latter value is implausible since at this redshift the bluest starlight feature (the Ca II absorption lines) should be apparent at $\lambda > 7450$ Å. Since the observed flux at this wavelength is $\sim 15 \times 10^{-16}$, the contribution of the host galaxy should be one-hundredth of this observed flux. This would imply the ability to detect spectral absorption with EW ~ 0.01 Å that is inconsistent with the spectral resolution and S/N of the presented data. Another clearly discrepant case is that of BZB J0915+2933, for which we give $z > 0.13$, while Shaw et al. reports $z > 0.53$. In this case, the source was a factor of ~ 5 fainter, which could help to detect the starlight component, but their S/N is visually worse ($\sim$30–50) than that of our spectra ($\sim$100–200), so the detection of the host-galaxy signature at $z \sim 0.5$ is very unlikely.

References

Ahnen, M. L., Ansoldi, S., Antonelli, L. A., et al. 2016, A&A, 595, A98
Álvarez Crespo, N., Masetti, N., Ricci, F., et al. 2016, AJ, 151, 32
Archambault, S., Archer, A., Benbow, W., et al. 2016, AJ, 151, 142
Archambault, S., Arlen, T., Aune, T., et al. 2013, ApJ, 776, 69
Bach, U., Raiteri, C. M., Villata, M., et al. 2007, A&A, 464, 175
Bade, N., Beckmann, V., Douglas, N. G., et al. 1998, A&A, 334, 459
Browne, I. W. A., Patnaik, A. R., Walsh, D., & Wilkinson, P. N. 1993, MNRAS, 263, L32
Cardelli, J. A., Clayton, G. C., & Mathis, J. S. 1989, ApJ, 345, 245
Carilli, C. L., Rupen, M. P., & Yanny, B. 1993, ApJL, 412, L59
Cepa, J., Aguiar-Gonzalez, M., Bland-Hawthorn, J., et al. 2003, Proc. SPIE, 4841, 1739
Cohen, J. G., Lawrence, C. R., & Blandford, R. D. 2003, ApJ, 583, 67
Danforth, C. W., Nalewajko, K., France, K., & Keeney, B. A. 2013, ApJ, 764, 57
Falomo, R., & Kotilainen, J. K. 1999, A&A, 352, 85
Falomo, R., Pian, E., & Treves, A. 2014, A&ARv, 22, 73
Finke, J. D., Shields, J. C., Böttcher, M., & Basu, S. 2008, A&A, 477, 513
Fischer, J.-U., Hasinger, G., Schwope, A. D., et al. 1998, AN, 319, 347
Fleming, T. A., Green, R. F., Jannuzi, B. T., et al. 1993, AJ, 106, 1729
Furniss, A., Williams, D. A., Danforth, C., et al. 2013, ApJL, 768, L31
Giommi, P., Piranomonte, S., Perri, M., & Padovani, P. 2005, A&A, 434, 385
Healey, S. E., Romani, R. W., Cotter, G., et al. 2008, ApJS, 175, 97
Henstock, D. R., Browne, I. W. A., Wilkinson, P. N., & McMahon, R. G. 1997, MNRAS, 290, 380
Jackson, N., Xanthopoulos, E., & Browne, I. W. A. 2000, MNRAS, 311, 389
Kinney, A. L., Calzetti, D., Bohlin, R. C., et al. 1996, ApJ, 467, 38
Kotilainen, J. K., Hyvönen, T., Falomo, R., Treves, A., & Uslenghi, M. 2011, A&A, 534, L2
Landoni, M., Falomo, R., Treves, A., et al. 2012, A&A, 543, A116
Landoni, M., Falomo, R., Treves, A., et al. 2013, AJ, 145, 114
Landoni, M., Falomo, R., Treves, A., & Sbarufatti, B. 2014, A&A, 570, A126
Landoni, M., Falomo, R., Treves, A., Scarpa, R., & Reverte Payá, D. 2015, AJ, 150, 181
Laurent-Muehleisen, S. A., Kollgaard, R. I., Ciardullo, R., et al. 1998, ApJS, 118, 127
Lawrence, C. R., Pearson, T. J., Readhead, A. C. S., & Unwin, S. C. 1986, AJ, 91, 494
Marcha, M. J. M., Browne, I. W. A., Impey, C. D., & Smith, P. S. 1996, MNRAS, 281, 425
Massaro, E., Giommi, P., Leto, C., et al. 2009, A&A, 495, 691
Massaro, F., Landoni, M., D'Abrusco, R., et al. 2015, A&A, 575, A124
Massaro, F., Masetti, N., D'Abrusco, R., Paggi, A., & Funk, S. 2014, AJ, 148, 66
Massaro, F., Paggi, A., Errando, M., et al. 2013, ApJS, 207, 16
Meisner, A. M., & Romani, R. W. 2010, ApJ, 712, 14
Miller, J. S., French, H. B., & Hawley, S. A. 1978, in Pittsburgh Conference on BL Lac objects, ed. A. M. Wolfe (Pittsburgh, PA: Univ. of Pittsburgh), 176
Morris, S. L., Stocke, J. T., Gioia, I. M., et al. 1991, ApJ, 380, 49
Nass, P., Bade, N., Kollgaard, R. I., et al. 1996, A&A, 309, 419
Nilsson, K., Pursimo, T., Heidt, J., et al. 2003, A&A, 400, 95
Nilsson, K., Pursimo, T., Sillanpää, A., Takalo, L. O., & Lindfors, E. 2008, A&A, 487, L29
Nilsson, K., Pursimo, T., Villforth, C., et al. 2012, A&A, 547, A1
Paiano, S., Landoni, M., Falomo, R., Scarpa, R., & Treves, A. 2016, MNRAS, 458, 2836
Patnaik, A. R., Browne, I. W. A., King, L. J., et al. 1993, MNRAS, 261, 435
Perlman, E. S., Stocke, J. T., Schachter, J. F., et al. 1996, ApJS, 104, 251
Piranomonte, S., Perri, M., Giommi, P., Landt, H., & Padovani, P. 2007, A&A, 470, 787
Plotkin, R. M., Anderson, S. F., Brandt, W. N., et al. 2010, AJ, 139, 390
Plotkin, R. M., Anderson, S. F., Hall, P. B., et al. 2008, AJ, 135, 2453
Rector, T. A., & Stocke, J. T. 2001, AJ, 122, 565
Rector, T. A., Stocke, J. T., Perlman, E. S., Morris, S. L., & Gioia, I. M. 2000, AJ, 120, 1626
Ricci, F., Massaro, F., Landoni, M., et al. 2015, AJ, 149, 160
Rovero, A. C., Muriel, H., Donzelli, C., & Pichel, A. 2016, A&A, 589, A92
Sbarufatti, B., Ciprini, S., Kotilainen, J., et al. 2009, AJ, 137, 337
Sbarufatti, B., Falomo, R., Treves, A., & Kotilainen, J. 2006a, A&A, 457, 35

Sbarufatti, B., Treves, A., & Falomo, R. 2005a, ApJ, 635, 173
Sbarufatti, B., Treves, A., Falomo, R., et al. 2005b, AJ, 129, 559
Sbarufatti, B., Treves, A., Falomo, R., et al. 2006b, AJ, 132, 1
Scarpa, R., Urry, C. M., Falomo, R., et al. 1999, ApJ, 521, 134
Scarpa, R., Urry, C. M., Padovani, P., Calzetti, D., & O'Dowd, M. 2000, ApJ, 544, 258
Schachter, J. F., Stocke, J. T., Perlman, E., et al. 1993, ApJ, 412, 541
Shaw, M. S., Romani, R. W., Cotter, G., et al. 2013, ApJ, 764, 135
Stickel, M., & Kuhr, H. 1993, A&AS, 101, 521
Tavecchio, F., Roncadelli, M., & Galanti, G. 2015, PhLB, 744, 375
Urry, C. M., Scarpa, R., O'Dowd, M., et al. 2000, ApJ, 532, 816
van Dokkum, P. G. 2001, PASP, 113, 1420
Wei, J. Y., Xu, D. W., Dong, X. Y., & Hu, J. Y. 1999, A&AS, 139, 575
Weistrop, D., Shaffer, D. B., Hintzen, P., & Romanishin, W. 1985, ApJ, 292, 614
White, R. L., Becker, R. H., Gregg, M. D., et al. 2000, ApJS, 126, 133
Wills, B. J., & Wills, D. 1974, ApJL, 190, L97
Wills, D., & Wills, B. J. 1976, ApJS, 31, 143
York, T., Jackson, N., Browne, I. W. A., Wucknitz, O., & Skelton, J. E. 2005, MNRAS, 357, 124
Zhu, G., & Ménard, B. 2013, ApJ, 770, 130